ISOTOPE EFFECTS ON THE OPTICAL SPECTRA OF GaP AND CdS

BY

THOMAS A. MEYER

HON. B. SC. CARLETON UNIVERSITY 1997

THIS THESIS SUBMITTED IN PARTIAL FULFILLMENT OF THE REQUIREMENTS FOR THE DEGREE OF MASTER OF SCIENCE IN THE DEPARTMENT OF PHYSICS

SIMON FRASER UNIVERSITY

DECEMBER 2003

APPROVAL

Name: Thomas A. Meyer

Degree: Master of Science

Title of Thesis: Isotope Effects on the Optical Spectra of GaP and CdS

Examining Committee:

Dr. Igor Herbut (Chair)
Associate Professor, Department of Physics

Dr. Michael Thewalt (Senior Supervisor)
Professor, Department of Physics

Dr. George Kirczenow (Supervisor)
Professor, Department of Physics

Dr. Simon Watkins (Supervisor)
Professor, Department of Physics

Dr. Michael Chen (Internal Examiner)
Senior Lecturer, Department of Physics

Date Approved: December 3, 2003

PARTIAL COPYRIGHT LICENSE

I hereby grant to Simon Fraser University the right to lend my thesis, project or extended essay (the title of which is shown below) to users of the Simon Fraser University Library, and to make partial or single copies only for such users or in response to a request from the library of any other university, or other educational institution, on its own behalf or for one of its users. I further agree that permission for multiple copying of this work for scholarly purposes may be granted by me or the Dean of Graduate Studies. It is understood that copying or publication of this work for financial gain shall not be allowed without my written permission.

Title of Thesis/Project/Extended Essay

Isotope Effects on the Optical Spectra of GaP and CdS

Author: _____
(signature)

Thomas A. Meyer
(name)

Dec. 9, 2003
(date)

ABSTRACT

The availability of samples of the binary compound semiconductors GaP and CdS with isotopically enriched gallium and sulfur composition respectively have allowed us to measure the change in the indirect band gap of GaP due to isotopic substitution of gallium and the change in the direct band gap of CdS due to isotopic substitution of sulfur. The technique of Fourier transform photoluminescence spectroscopy has been used to measure the fine structure of the sulfur donor-carbon acceptor pair band in samples of GaP with differing isotopic composition of gallium, resulting in a measurable shift of the fine structure spectra. In the CdS samples, photoluminescence and reflectivity spectroscopy have been used to measure the donor bound exciton spectrum and the free exciton spectrum, revealing a shift in the fine structure of these spectra between the samples of different isotopic composition of sulfur. These changes in bandgap are explained in the context of the renormalization of the electronic band gap due to the electron-phonon interaction.

Acknowledgements

I thank the SFU physics department and more specifically Dr. M.L.W. Thewalt and the Thewalt lab group for providing the means to scientific research.

Table of Contents

List of Tables

List of Figures

Chapter 1 : Introduction

The effects of isotopic composition on the properties of crystals is a study which has become a subject of great current interest. These effects have been summarized in many comprehensive reviews on the subject[1,2]. One of the more significant physical properties that is strongly affected by isotopic composition is thermal conductivity. Although this crystal property may be of greatest significance for the industrial applications of semiconductors, isotopic content also has a wide range of effects on other bulk and surface properties of semiconductors, which have proven to be of great significance for the scientific knowledge of semiconductors and of the physics of the solid state. Isotopic studies have had effects on the world of physics in as far ranging a manner as to become of great importance to the physics of metrology, where a recent study, *The Avogadro Project*[3] has been undertaken in hopes of a new realization of the SI unit of mass (kg) by the growth of high purity monoisotopic Si boules.

One of the bulk properties which is considered the most distinguishing feature of a given semiconductor is the electronic bandgap. Solid state theoreticians may estimate the bandgap of a given semiconductor using ab initio electronic band structure calculations. These calculations will produce an estimate within an accuracy of 100meV typically. However these calculations neglect the interaction of the electron with the vibrations of the host lattice, the electron-phonon interaction, with the assumption that the atoms of the host lattice occupy fixed positions. Taking this interaction into consideration, one calculates a contribution to the band gap which is termed the *electron-phonon renormalization* of the bandgap. This renormalization term is known to be dependent upon both temperature and the average isotopic mass of the host crystal.

In this thesis we present empirical measurements which give the dependence of the bandgaps of two binary compound semiconductors, GaP and CdS, upon the average isotopic mass of the constituent atoms of these crystals. We measure the dependence of the indirect gap of GaP on gallium isotopic composition and the dependence of the direct gap of CdS on sulfur isotopic composition.

In chapter 2 a brief introduction to the relevant theory is given, including an explanation of the crystal structure for each of GaP and CdS and an introduction to the optical spectra of each crystal. The theory relevant to the electron-phonon interaction and its effect on the electronic bandgap is also discussed. In Chapter 3 the experimental arrangement is discussed with an explanation of the related spectroscopy. The experimental results are discussed for GaP in chapter 4 and for CdS in chapter 5.

Chapter 2 : Theoretical Framework

2.1 Excitons

In the presence of photons whose energy is greater than the bandgap of the host crystal, an electron may be excited from its state in the valence band into a state in the conduction band. As a result, a hole will be left behind in the valence band. In the low temperature limit when thermal excitations are absent, the electron and hole may find it energetically favorable to bind together due to their Coulombic attraction, thus creating an *exciton*. The exciton will typically have a lifetime on the order of microseconds (in indirect bandgap material) and of nanoseconds (in direct bandgap material), and its decay is due to the recombination of the electron and hole whereby a photon of characteristic energy is emitted. The classification of excitons[4] is divided into those known as Frenkel excitons, whose spatial extent is on the order of the atomic spacing of the host lattice, and Wanier-Mott excitons, whose spatial extent is far greater than that of the atomic spacing. We will limit our discussion here to that of Wanier-Mott excitons, typical of semiconductors.

If the exciton is free to travel within the crystal, as for *free excitons*, then its recombination luminescence is a function of the bandgap energy, E_g, the kinetic energy of the exciton, E_k, and the Coulombic binding energy of the exciton in the state n, E_n,

$$E_{FE} = E_g + E_k - E_n \quad \text{with} \quad E_n = \frac{\mu e^4}{2\eta^2 \varepsilon^2 n^2}$$

where E_{FE} is the energy of the free exciton luminescence, E_n is an approximation of the Coulombic binding energy for the case of a non-degenerate isotropic conduction band, n = 1,2,...(n=1 is the ground state) is an integer, $\eta = 4\pi\varepsilon_o\hbar$, ε is the dielectric constant of the

host crystal and $\mu=(1/m_e^*+1/m_h^*)^{-1}$ is the reduced mass of the exciton with m_e^* and m_h^* the effective masses of the electron and hole respectively.

The electron which was excited by the absorption of a photon to a conduction band state returns to a valence band state by the emission of a photon of energy E_{FE}, when it recombines with the hole. In an indirect gap material, the energy of luminescence is also reduced by a wavevector-conserving phonon.

The presence of impurities and defects in the host crystal may trap the free exciton in a localized state. The free excitons will find it favorable to reduce their energy in the presence of a localizing potential. The energy of localization for the exciton, E_l, simply reduces the energy of the exciton. This is referred to as a *bound exciton* and it has recombination luminescence energy E_{BE} which is the same as that of the free exciton except without the kinetic energy term and minus the localization energy,

$$E_{BE} = E_g - E_n - E_l$$

This expression is not necessarily accurate for all excited states of the bound exciton as the exciton binding energy may take a different form due to the presence of the impurity. With the additional reduction in energy by the localizing potential, the bound exciton luminescence will be lower in energy than the free exciton luminescence.

We will only consider here excitons bound to neutral donor impurities. A donor impurity in a binary compound consists of an atom which has one more valence electron than the atom of the host crystal which it replaces. The term neutral simply implies that the extra electron of the donor impurity is in a bound state at the impurity, as opposed to an ionized donor impurity whose associated electron is free and in the conduction band.

Donor bound exciton luminescence is different from that of free exciton recombination luminescence in that the bound exciton, which may be in an excited state, undergoes recombination to leave behind a neutral impurity, which may also have its extra electron in an excited state. Thus the luminescence, which will have an energy of the difference in energy of the final and initial states, will have a number of varying characteristic energies dependent upon the initial ground or excited state of the bound exciton and the final ground or excited state of the neutral donor. This leads to a series of luminescence decay energies which are characteristic of the recombination of a donor bound exciton.

2.2 Excitonic-Polaritons

In this section we will present a limited description outlining the features relevant to this thesis, but the interested reader is directed to a much more in-depth description in the literature[5]. The excitonic-polariton(EP) is composed of a photon coupled to a free exciton. In the case of broad band light incident upon a crystal, if the frequency range of the light covers the resonance region of the EP, then the EP modes will be excited. The EP is confined to the interior of the crystal which is bounded by an exterior region of reflected/scattered light radiation. The matching of interior and exterior fields at the boundary is the essence of the EP problem.

By matching the exterior fields to the interior fields with appropriate boundary conditions, one can calculate the reflectivity in the resonance region of the EP. The reflectivity will be changed in the resonance region of the EP in such a way that the reflectivity will locally have a maximum and minimum. This is seen in Fig 2.1 where a reflectance spectra of the free exciton region in CdS is displayed.

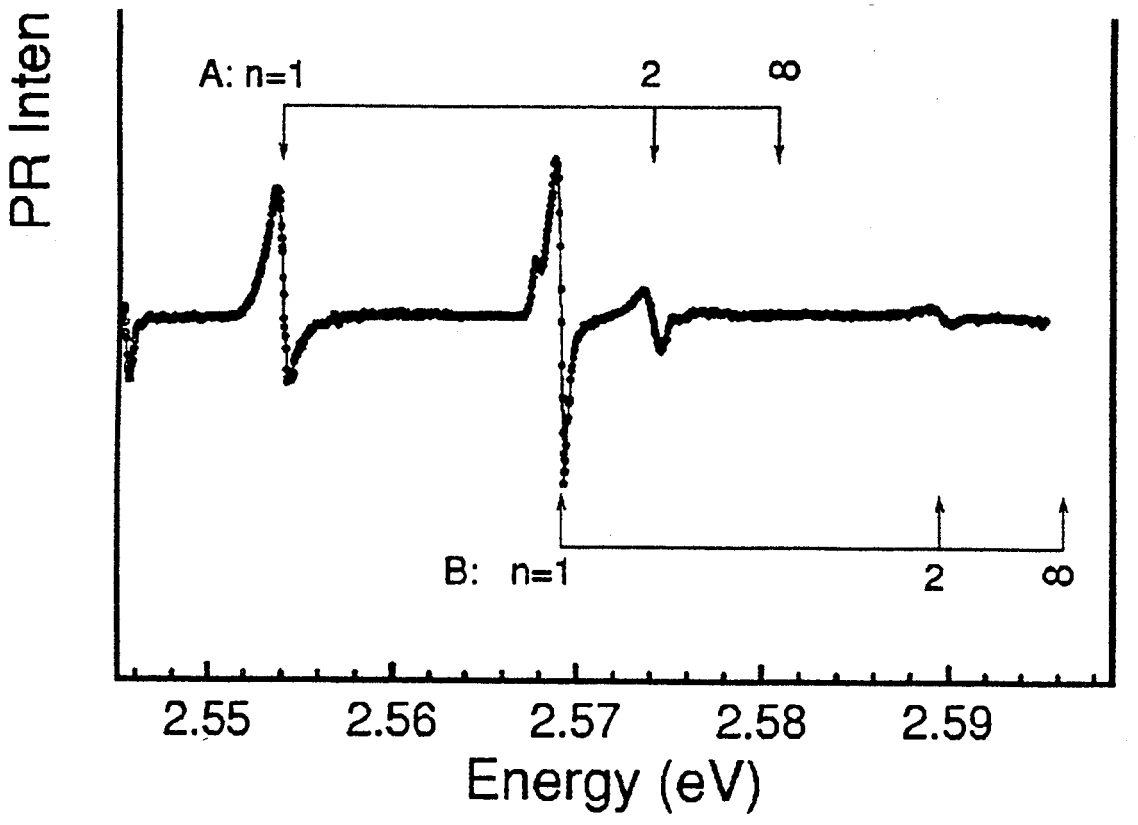

Figure 2.1 Photomodulated reflectivity spectrum of CdS at 6K from Ref. 21. Assignment of spectral features to components of the series of A and B excitons is indicated.

2.3 Donor Acceptor Pair Recombination

The thermal equilibrium state of conduction and valence band occupancy predicts that for a semiconducting crystal with donor and acceptor concentrations N_D and N_A, if the crystal is n-type such that $N_D > N_A$, then there will be N_A ionized donors and acceptors and N_D-N_A neutral donors. This however, will only hold under equilibrium conditions and for temperatures low enough such that $kT \ll E_D, E_A$, where E_D and E_A are the binding energy of the donor and acceptor impurities respectively, since at room temperature essentially all donors and acceptors will be ionized. In the event that light of energy greater than the bandgap of the crystal is incident upon the crystal, electrons from the valence band will be promoted to the conduction band by the absorption of photons, thus leaving behind holes in the valence band. These excess electrons will predominantly be trapped by the ionized donors and most of the excess holes will be trapped by the ionized acceptors. The result is a natural tendency back towards the equilibrium state via radiative electron-hole recombination. This process is what has been termed as *donor acceptor pair recombination luminescence.*

The theoretical framework of donor acceptor pair (DAP) recombination has been well documented[6,7] with much of the pioneering experimental work being done with GaP crystals. The DAP luminescence we will be treating here is for a zinc blende crystal structure of a binary compound semiconductor, which is composed of two interpenetrating fcc lattices where the anion atoms sit on one lattice and the cation atoms sit upon the other. This DAP luminescence is further categorized into two types which differentiate between the substitutional placement of the donor and acceptor atoms on the zinc blende structure. Type I DAP luminescence has both donor and acceptor atoms

occupying substitutional sites upon the same fcc lattice and Type Π with donor and acceptor atoms occupying substitutional sites on separate fcc lattices of the zinc blende structure.

In this thesis we will be specifically dealing with the Type I DAP luminescence of GaP crystals due to the presence of C and S impurities, where carbon is a substitutional acceptor on the phosphorous lattice sites and sulfur is a substitutional donor on the phosphorous lattice sites.

The energy of a specific DAP transition, E_{DAP}, is a function of the distance of separation between the donor and acceptor, **r**, and it can be approximated as,

$$E_{DAP} = E_g - E_D - E_A + \frac{e^2}{\varepsilon r}$$

If the donor and acceptor concentrations are very low, then very few *pairs* of donors and acceptors will have small **r**, and the luminescence of pairs with different **r** will all blend into a band. If donor and acceptor concentrations are fairly high, then there will be a significant number of pairs with small **r**, where the difference in Coulomb energy from one **r** to the next is large enough that the luminescence of pairs with different **r** will be well resolved. This is referred to as *discrete* DAP luminescence.

This expression for E_{DAP} is only an approximation, and the energies of transition for different **r** may not be accurately predicted with its use.

The enumeration of distances between donors and acceptors for Type I zinc blende DAP bands has been calculated by several authors[6,8,9] and will be presented in the same formalism as in the literature.

The fine structure of a DAP luminescence band is determined by the distance of separation of the donor and acceptor. This radial distance will be assumed to have its origin at one of the atomic sites at the corner of an fcc lattice cell. The calculation of the distance of separation can be further understood with reference to the sub-lattices of Fig 2.2. The fcc lattice can be broken into sub-lattices of type sc(simple cubic) and fc(face-centered) as in Fig 2.2. It is noted that if one measures **r** in units of a/2 where a is the lattice constant of the zinc blende crystal, then

$$\boldsymbol{r} = u\boldsymbol{a}_1 + v\boldsymbol{a}_2 + w\boldsymbol{a}_3$$

where $\boldsymbol{a}_1, \boldsymbol{a}_2, \boldsymbol{a}_3$ are rectangular basis vectors of the crystal similarly measured in units of a/2 and u, v, w are integers. So now

$$r^2 = u^2 + v^2 + w^2$$

is the relation which gives r in terms of $\langle u,v,w \rangle$ where conditions on these integers will allow us to express r^2 in terms of a shell index, m=1,2,3... This index corresponds to the concentric shells of radius r which have the possible positions of the other member of the pair at lattice sites within the surface of the shell.

For the fc(face-centered) sub-lattice it is noted that the set of $\langle u,v,w \rangle$ must have two odd integers and one even in order that the relation for **r** reproduce the sites of the fc sub-lattice. The criterion for $\langle u,v,w \rangle$ in the sc(simple-cubic) sub-lattice is that all three must be even. Both criteria can be summarized in the following relation which must hold for the total fcc lattice,

$$u + v + w = even$$

It is also noted that since there are two odd and one even of the three integers, then the squares of the three integers are also two odd and one even. This leads to the criterion

$$r^2 = u^2 + v^2 + w^2 = even = 2 \times Integer$$

If we simply assign the integer in this relation as m, our shell index integer, then we have the desired relation between r and m,

$$r_m = \sqrt{\frac{m}{2}}a$$

Taking this relation into account, the enumeration of DAP radial separations r_m is performed by Dean[6] as given in Table 2.1. The degeneracy number indicates the number of different lattice sites at that distance due to symmetry of the crystal.

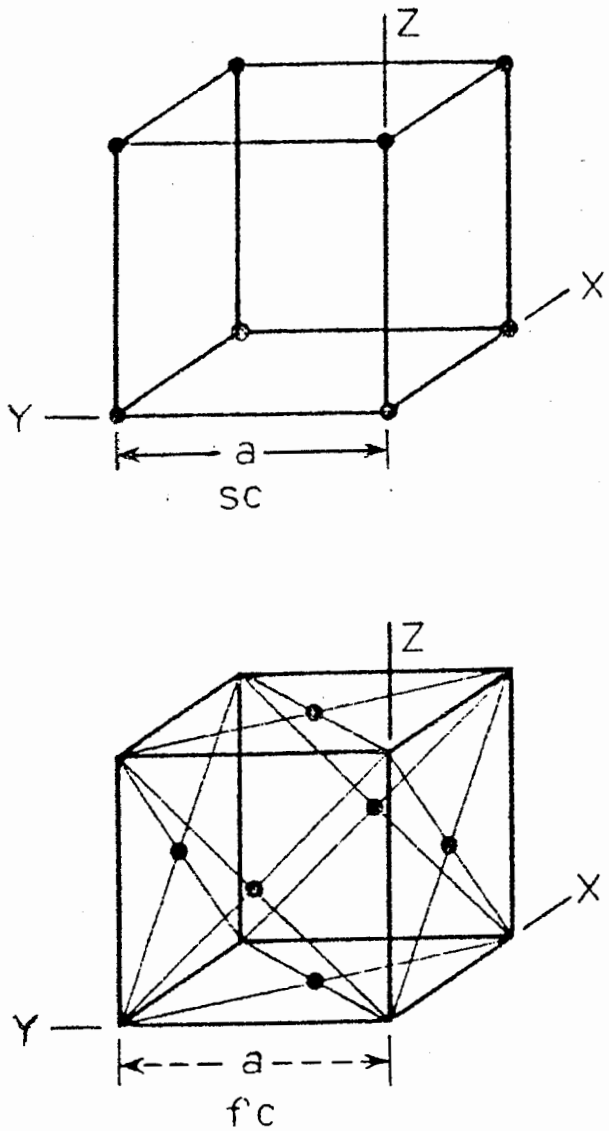

Figure 2.2 The sublattices of the fcc(face-centered cubic) lattice. The sc(simple cubic) and fc(face centered) sub-lattices together make up the fcc lattice (fcc = sc + fc).

Table 2.1 Enumeration of r_m for a Zincblende Type I DAP Band

Shell Number (m)	Lattice Vector <u,v,w> unit a/2	Degeneracy[+]
1	<1,1,0>	12
2	<2,0,0>	6
3a,b	<2,1,1>*	12
4	<2,2,0>	12
5	<3,1,0>	24
6a,b	<2,2,2>*	4
7a,b	<3,2,1>*	24
8	<4,0,0>	6
9a,b	<4,1,1>*	12
9c	<3,3,0>	12
10	<4,2,0>	24
11	<3,3,2>*	12
12	<4,2,2>*	12
13a	<5,1,0>	24
13b,c	<4,3,1>*	24
15a,b	<5,2,1>*	24

Denote inverse sets. For each set <u,v,w> there is an equivalent inverse set due to inversion symmetry with equal degeneracy. (a,b,c) distinguish multiple sets of similar m.

[+]The determination of the degeneracy number goes as follows. The degeneracy number is 24 if u,v,w are all different, 12 if two are equal but non-zero and 6 if two are zero.

2.4 The GaP Crystal

The GaP crystal has a zinc blende lattice structure composed of two interpenetrating face-centered-cubic lattices with Ga atoms sitting on the points of one lattice and P atoms sitting at the lattice points of the other. The crystal structure has the second lattice positioned at the basis (1/4,1/4,1/4) along the diagonal as shown in Fig. 2.3(a). The first Brillouin zone of the zinc blende reciprocal lattice is shown in Fig. 2.3(b). In the band structure of GaP it turns out that the valence band maximum is centered at the Γ point and the conduction band minimum is at a point along the Δ axis near the X point of the zone boundary. This being the case, the conduction band minimum is not directly aligned with the valence band maximum, thus GaP is an indirect gap semiconductor. This being the case, the GaP crystal does not exhibit luminescence as strongly as with a direct gap material.

(a)

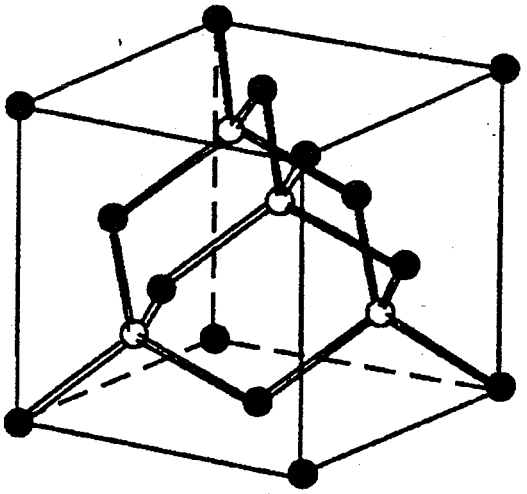

Zn

S

(b)

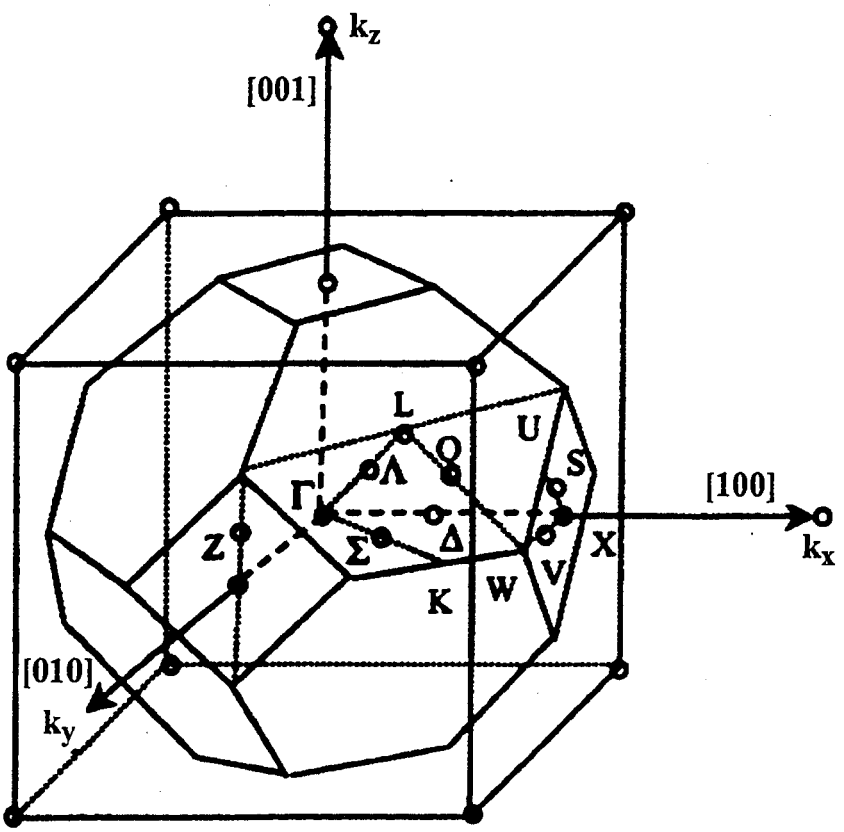

Figure 2.3 Lattice structure (a) of the zinc blende crystal lattice and the first Brillouin zone (b) of the zinc blende lattice.

(a)

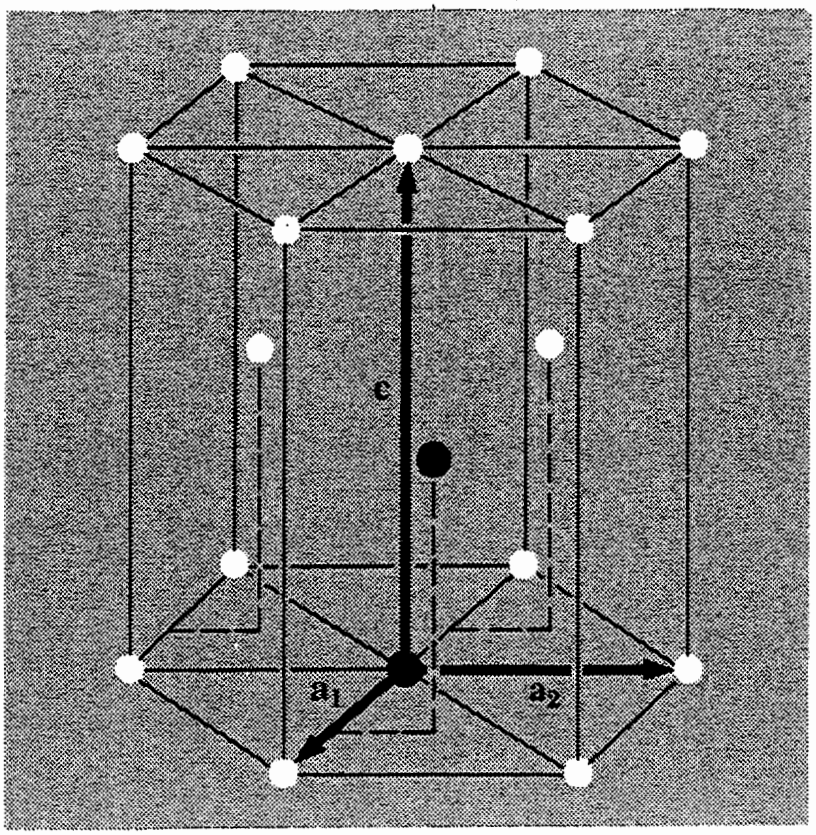

(b)

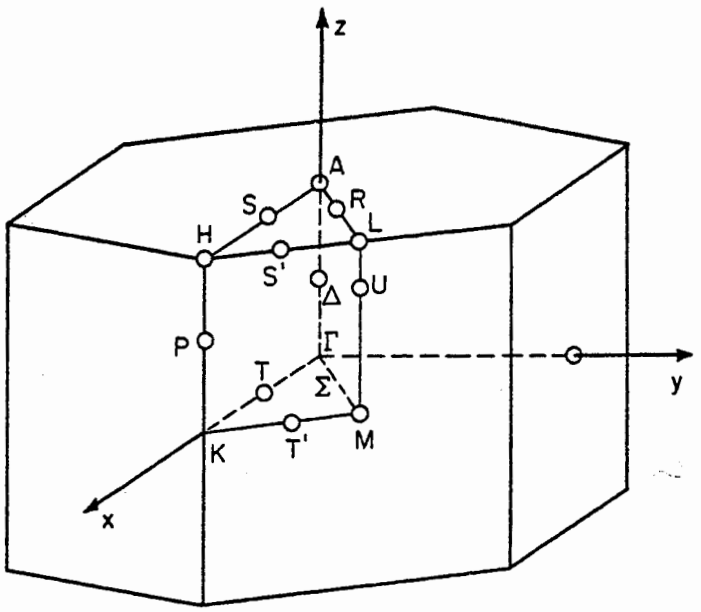

Figure 2.4 Lattice structure(a) of the wurzite type crystal lattice with solid circles indicating basis atoms and the first Brillouin zone (b) of the wurzite lattice.

2.5 The CdS Crystal

The CdS crystal has a wurzite or hexagonal-close-packed crystal lattice structure composed of two interpenetrating hexagonal lattices with a basis (2/3,1/3,1/2) as shown in Fig. 2.4(a). The first Brillouin zone of the wurzite reciprocal lattice is shown in Fig. 2.4(b). The point group for the hexagonal lattice at the Brillouin zone center is D_{6h} in Koster notation. The character table for the D_{6h} point group is given in Table 2.2.

For CdS it turns out that the conduction band minima and the valence band maxima are both centered at the Γ-point of the Brillouin zone such that CdS is a direct gap semiconductor. The valence band of CdS results from the 3p states of sulfur and is split due to crystal-field splitting and spin-orbit coupling such that it has three nearly degenerate valence band maxima at the Γ-point resulting from the three sub-bands referred to as A, B and C in the literature. The A band has Γ_9 symmetry, whereas the B and C bands have Γ_7 symmetry. The conduction band results from the 5s states of cadmium and has Γ_7 symmetry.

For free excitons which have the constituent electron in a conduction band state and the corresponding hole in a valence band state, the final state of the exciton will have symmetry which may be found by the decomposition of the group symmetries of the valence and conduction bands. Since the A sub-band differs in symmetry from the B and C sub-bands, then the recombination luminescence transitions which occur between the conduction band and these three sub-bands will differ in symmetry as well. For excitons composed of a hole in a state of the A sub-band of the valence band, A excitons, the group representation may be decomposed as $\Gamma_{9v} \times \Gamma_{7c} = \Gamma_5 + \Gamma_6$ where subscripts v and c correspond to valence and conduction band respectively. For B and C excitons the

decomposition goes as $\Gamma_{7v} \times \Gamma_{7c} = \Gamma_1 + \Gamma_2 + \Gamma_5$. If the polarization of the emitted light is such that $\mathbf{E} \| \mathbf{c}$, where $\mathbf{c}$ is the hexagonal crystal axis, then transitions are allowed to the Γ_1 states. For polarization $\mathbf{E} \perp \mathbf{c}$, transitions to Γ_5 states are allowed[21].

2.6 Spectroscopy

In this thesis we will present results which were obtained by two different methods of spectroscopy; photoluminescence and reflectance spectroscopy. Photoluminescence involves the process of exciting the electrons of a crystal via incident light with energy in excess of the bandgap energy. The excited states of the electrons and holes will only last a small amount of time, after which the de-excitation results in the emission of photons of characteristic energy. By measuring the energy of the emitted light, one learns more about the excited state properties of the electrons and holes for the given host crystal.

We are looking at exciting CdS crystals with laser light of energy greater than the direct band gap of the crystal in order to excite electrons into the conduction band. This is done at low temperatures of ~1.3K such that the electrons and holes may create free excitons, of which some will become bound to neutral impurities. Then the de-excitation process comes in the form of electron-hole recombination for which there is luminescence of characteristic energy as explained in section 2.1.

For GaP crystals, we will complete the same experimental process. However, we will observe the luminescence, not in the excitonic region, but in the region of the donor acceptor pair band luminescence which has also been discussed in section 2.3.

For CdS crystals, we will also use reflectance spectroscopy in the region of the free exciton energies. This involves directing incident light on the crystal of a wide energy range which will cover the whole excitonic region of interest. This will excite the various

excitonic-polaritons associated with the free excitons of CdS. This will then accordingly modify the intensity of reflected light at the polariton resonance energies. By analyzing the reflected light we will recover information about the characteristic energies of the excitonic-polaritons.

E	C_2	$2C_3$	$2C_6$	$3C_2'$	$3C_2''$	I	σ_h	$2S_6$	$2S_3$	$3\sigma_v$	$3\sigma_d$
1	1	1	1	1	1	1	1	1	1	1	1
1	1	1	1	-1	-1	1	1	1	1	-1	-1
1	-1	1	-1	1	-1	1	-1	1	-1	1	-1
1	-1	1	-1	-1	1	1	-1	1	-1	-1	1
2	-2	-1	1	0	0	2	-1	-1	1	0	0
2	2	-1	-1	0	0	2	2	-1	-1	0	0
1	1	1	1	1	1	-1	-1	-1	-1	-1	-1
1	1	1	1	-1	-1	-1	-1	-1	-1	1	1
1	-1	1	-1	1	-1	-1	1	-1	1	-1	1
1	-1	1	-1	-1	1	-1	1	-1	1	1	-1
2	-2	-1	1	0	0	-2	2	1	-1	0	0
2	2	-1	-1	0	0	-2	-2	1	1	0	0

Table 2.2 Character table for the point group D_{6h}.

2.7 Isotopic Dependence of the Bandgap

The electronic bandgap, which is the energy difference between the minimum of the conduction band and the maximum of the valence band, is what distinguishes a semiconductor from an insulator. Semiconductors have bandgaps on the order of eV whereas insulators typically have much larger bandgaps.

As mentioned in the introduction, typical band structure calculations for a given crystal will lead to an estimate of the bandgap accurately within 100 meV. However, various techniques of measuring the bandgap experimentally have proven to give accuracies on the order of meV. The direct bandgap of CdS due to the A valence band has been measured[10] as 2.5827eV and the indirect band gap of GaP has been measured[11] as 2.346eV. Both of these measurements were taken at temperatures of interest in this thesis (1.3K).

With this accuracy of the measurements of the electronic bandgap, one becomes interested in perturbations that might change the bandgap in a measurable fashion. One characteristic that has a small yet ascertainable effect is isotopic mass. In recent years, it has been found that the bandgap is renormalized by the electron-phonon interaction[1,12]. This renormalization has a definite effect that may be understood with reference to the *raw* bandgap. The raw bandgap is that which would be calculated without including consideration of the electron-phonon interaction, i.e. the bandgap in the absence of lattice vibrations. We will refer to the actual bandgap of a material as E_g. The difference between the raw bandgap and the actual bandgap is the renormalization, ΔE_g, which is

due to the electron-phonon interaction. The renormalization term is a temperature dependent quantity. We will find its temperature dependence as follows.

The renormalization in first order is known[1] to be proportional to the average of the squared amplitude of vibration of the constituent atoms, $\langle u^2 \rangle$. It should be noted at this point that the band gap renormalization is also affected by the temperature directly, via thermal expansion[1]. This thermal expansion contribution to the change in the bandgap has a similar dependence upon $\langle u^2 \rangle$, so we will treat the two contributions to the renormalization as though they were one.

The average squared amplitude is related to the Bose-Einstein statistical factor, n_B, as

$$\left\langle u^2 \right\rangle = \left\langle \frac{\hbar}{4M\omega}(2n_B + 1) \right\rangle$$

where M is the average isotopic mass of the atoms of the host crystal, ω is the phonon frequency and

$$n_B = \frac{1}{e^{\frac{\hbar\omega}{k_B T}} - 1}$$

The brackets <...> imply an average over all phonon modes, which may be equivalently performed by substituting for the phonon frequency with the Debye frequency, ω_D. The low and high temperature limits are then found as,

$$\mathrm{T} \to 0 \qquad \Delta E_g \propto \left\langle u^2 \right\rangle = \frac{\hbar}{4M\omega_D}$$

$$\mathrm{T} \to \infty \qquad \Delta E_g \propto \left\langle u^2 \right\rangle = \frac{k_B T}{2M\omega_D{}^2}$$

The angular frequency of a phonon which corresponds to a given wavevector $\boldsymbol{k}$ and branch j in the harmonic approximation is known to have dependence upon isotopic mass[1] as,

$$\omega_{j,k} = \sqrt{\frac{f(j,k)}{M}} \propto M^{-\frac{1}{2}}$$

where $f(j,\mathbf{k})$ is a restoring force constant. This expression can be used to substitute for ω_D. This will give us limits of the band gap renormalization as

$$\mathrm{T} \rightarrow 0 \qquad \Delta E_g \propto M^{-\frac{1}{2}}$$

$$\mathrm{T} \rightarrow \infty \qquad \Delta E_g \propto T$$

At low temperatures, the zero-point renormalization of the bandgap can be as much as 100meV. At the lowest temperatures, the renormalization is expected to be independent of temperature. In the high temperature limit, the dependence on isotopic mass fades and the renormalization has a linear dependence upon the temperature.

Chapter 3 : The Experiment

3.1 Fourier Transform Spectroscopy

Fourier Transform spectroscopy is a form of spectroscopy which is non-spatially-dispersive. This means that unlike other forms of spectroscopic analysis, it does not spatially separate the different frequencies of radiation in order to acquire spectral information. It uses a Fourier transform of the output from a traveling Michelson interferometer. The basic setup of this interferometer is illustrated in Fig3.1. The input beam coming from the source is incident upon the beam splitter. The beam splitter simply divides the radiation beam into two equal beams, one reflected and one transmitted. The transmitted beam is then reflected back to the beam splitter by a traveling mirror, M_2, and the reflected beam is reflected back by a fixed mirror, M_1. Both beams are then incident upon the detector. The two beams are now out of phase from one another due to a difference in the optical path length so when they are recombined the output intensity goes as,

$$I_{out}(x) = \frac{I_{in}}{2} + \int_{-\infty}^{\infty} \frac{B(v)}{2} \cos(2\pi v t) dv$$

where $I_{out}(x)$ is the intensity of the output interference beam, I_{in} is the intensity of the input beam, $B(v)$ is the amplitude of the component of the output with frequency v and x is the optical path retardation($x=c\tau$ where τ is the difference in time propagation of the two beams and c is the velocity of light). But we seek to find the spectral information which is given by $B(v)$, so we must perform an inverse cosine Fourier transform,

$$B(v) = 2\int_{-\infty}^{\infty} C(\tau)\cos(2\pi v\tau) d\tau$$

where $C(\tau) = I_{out} - I_{in}/2$. The interferometer simply collects the intensity as a function of optical path retardation, called the *interferogram*, and a computer calculates the Fourier transform and returns the spectral information of intensity as a function of wavenumber.

3.2 Dispersive Spectroscopy Using Diffraction Gratings

The typical reflection grating is made with one surface modified in such a manner that many long parallel grooves of a definite spacing are permanently marked into it. Any light scattered from the periodic surface features will have a phase relationship in accordance with the spacing of the grooves. This type of grating is referred to as a *reflection phase grating*. The equation for this grating can be obtained[13] from the analysis of two emergent scattered beams from the reflection off the grating as in Fig3.2. The two emergent beams are scattered from adjacent grooves. If the two emergent beams are to be collimated and in phase, then the optical path difference which they undergo must be an integral multiple of wavelengths of the light. From the figure we can see that the optical path difference is given as $AB\text{-}CD = a(\sin\theta_m\text{-}\sin\theta_i)$ such that the equation of the grating is

$$m\lambda = a(\sin\vartheta_m - \sin\vartheta_i)$$

where a is the grating spacing, θ_i is the incident angle of the luminescence radiation and θ_m is the angle of reflection for the m^{th} order reflection. The order m must be an integer.

In total then, the grating simply disperses the light such that different frequencies of light will be reflected at different angles and this is then repeated over great angles of separation for the different orders of integer m.

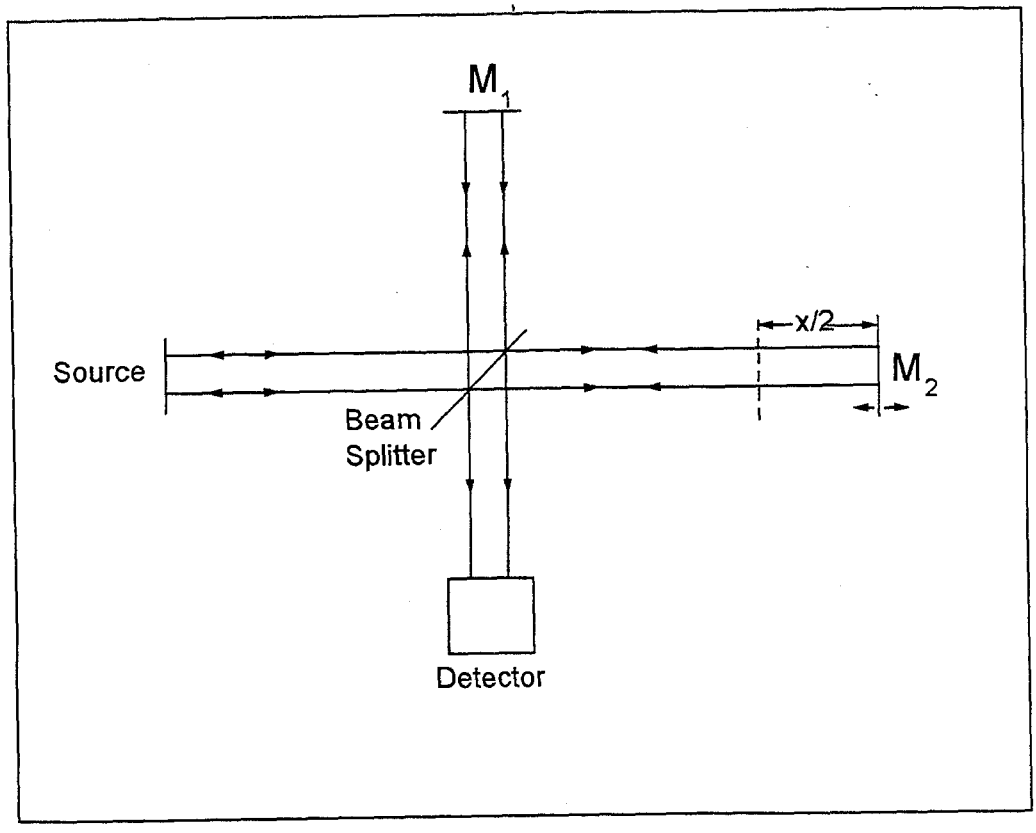

Figure 3.1 A Michelson Interferometer

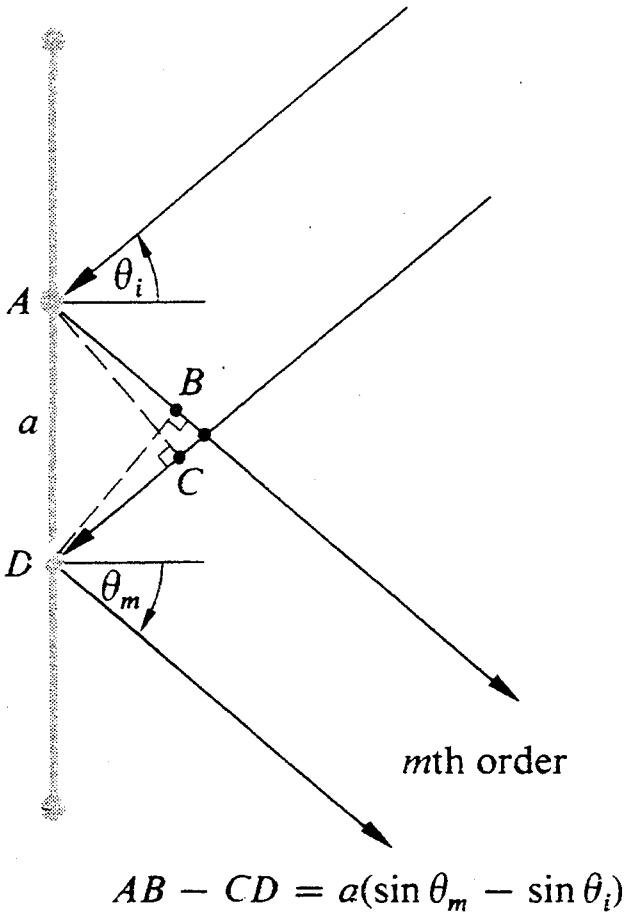

Figure 3.2 A reflection grating

3.3 Experimental Arrangement

3.3.1 Setup

The essential elements of the experimental setup for photoluminescence and reflectance spectroscopy consist of the semiconducting material samples, a He cryostat, a source of above-band-gap light, an instrument for spectroscopic analysis and an appropriate radiation detector. Of course, any lab equipped to do this spectroscopy will also be furnished with all the associated optical equipment and electronics for monitoring purposes. For all photoluminescence experiments, the excitation source used is an Argon ion laser with wavelength 457.9nm. For all reflectivity experiments, the light source used was a tungsten lamp.

In this thesis we will present findings which were acquired from two different experimental arrangements. The difference between the two arrangements is the instrument used for analysis and the radiation detector used. In one setup, Fourier transform spectroscopy is performed with the use of a Bomem DA8 interferometer and a Si photodiode detector. In the other setup, a reflection grating is used for analysis and a charge coupled device (CCD) detection system is used. Both systems will be explained below.

3.3.2 Bomem DA8

The setup is illustrated in Fig.3.3 where it is seen that the samples are placed in the ^{4}He cryostat (dewar) where the excitation laser light is incident upon the samples and the resulting luminescence radiation is collimated by a parabolic mirror. The collimated radiation beam is then analyzed by a traveling Michelson interferometer. The beam is first reflected off a fixed mirror and then incident upon the beam splitter. The beam

splitter returns the interference beam toward the variable aperture. The interference beam which exits the aperture is then filtered to eliminate any stray room light or excitation laser light and pass only the luminescence of interest. The remaining beam is then incident upon the detector. The internal source of light can be directed along the optical path in the opposite direction so that it exits at the sample, where it can be focused. By focusing the internal light on the sample, the optical path is adjusted to receive luminescence from the sample.

3.3.3 Reflection Grating Spectrometer

The excitation laser and ^{4}He dewar setup are the same as they were with the Bomem setup. The setup of the reflection grating spectrometer is illustrated in Fig3.4 where it is seen that the luminescence radiation is focused by a spherical lens onto an entrance slit through a shutter. The shutter is opened for the amount of time intended for the exposure. When the shutter is open, the radiation is focused at the entrance slit which has width 100μm. The beam then travels to a spherical mirror which is separated from the slit by a distance equal to the focal length of the mirror. The mirror then reflects the collimated beam onto the reflection grating. The diffracted light is now separated into various orders in accordance with the equation of the grating. The m=-4 order is selected out by a spherical mirror and directed toward the CCD screen. The reflection grating used is a Milton Roy Company grating with a groove spacing of 600 grooves/mm. The CCD system used is a Photometrics SDS9000 CCD detector system.

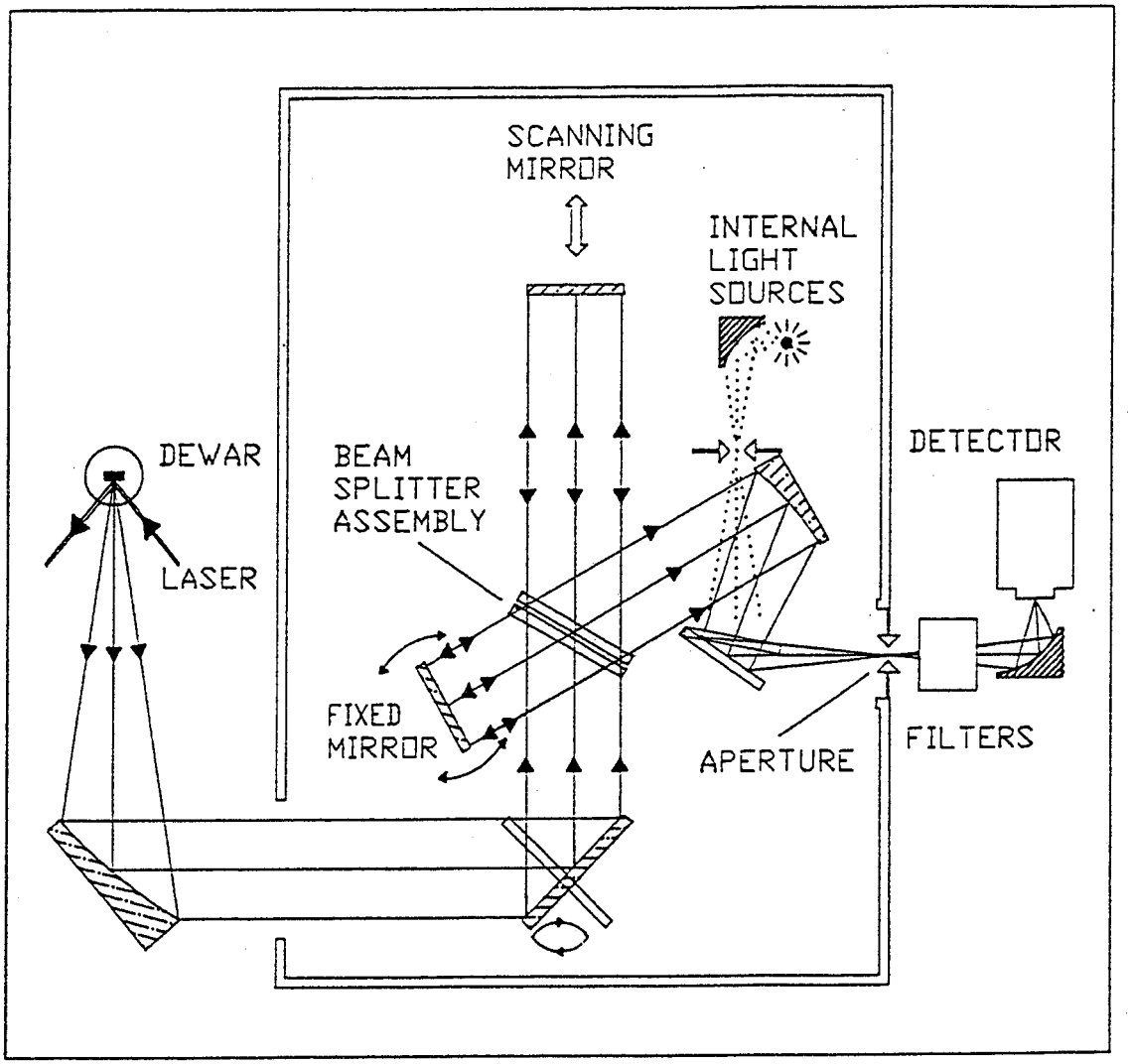

Figure 3.3 The Bomem DA8

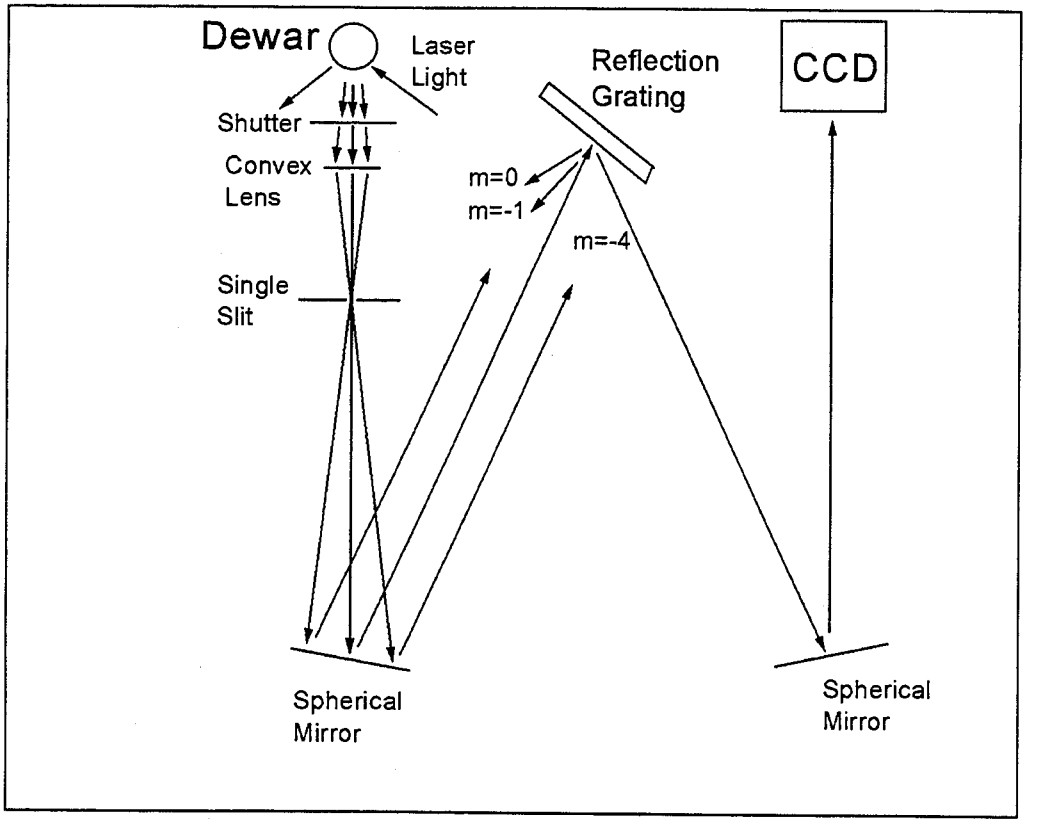

Figure 3.4 Reflection Grating Spectrometer

3.3.4 Samples

The GaP samples were unoriented bulk crystal grown from Ga-P solution at 1340K with typical dimensions of several hundred microns. The four crystals will be referred to with superscripts indicating the average isotopic mass of gallium. The crystal with lightest Ga mass is ^{69}GaP with isotopic composition of 99.5% ^{69}Ga and 0.5% ^{71}Ga which gives average isotopic mass <M>=68.926amu. The second lightest is ^{nat}GaP with composition 69.6% ^{69}Ga and 30.4% ^{71}Ga which gives <M>=69.533amu. The superscript *nat* implies that this sample has gallium isotopic composition close to that of natural gallium. Natural gallium has ^{69}Ga and ^{71}Ga with percentage abundances of 60% and 40% respectively. The next heavier crystal is ^{anti}GaP with composition 40% ^{69}Ga and 60% ^{71}Ga which gives <M>=70.125amu. The *anti* superscript indicates that this is the so-called 'anti-natural' gallium which has percentage abundances reversed from that of natural gallium. The crystal with the greatest Ga mass is ^{71}GaP which has 0.5% ^{69}Ga and 99.5% ^{71}Ga which gives average isotopic mass of gallium as <M>=70.925amu.

The samples were grown from vapour transport using natural Cd and either of natural sulfur or isotopically enriched ^{34}S. The samples had a long thin platelet shape with the hexagonal c axis lying in the surface of the platelet parallel to the longer side.

Sulfur has four stable isotopes, ^{32}S, ^{33}S, ^{34}S and ^{36}S, and the percentage abundance of these isotopes in natural sulfur is 95.02%, 0.75%, 4.21% and 0.02% respectively. This gives an average isotopic mass of natural sulfur as <M>= 32.0625amu.

The other sample was isotopically enriched with ^{34}S and it had percentage composition of 99% ^{34}S, 0.9% ^{33}S and 0.1% ^{32}S. This gives an average isotopic mass of sulfur as <M>=33.957amu.

Chapter 4 : GaP Results

4.1 Photoluminescence

Photoluminescence spectra were collected from all four samples in the region of the DAP band due to S and C impurities in GaP. Fine structure lines of the DAP band were found to be abundant and consistent between the different samples. In Fig 4.1 the spectra with lines due to the m=10 to m=15 shells is displayed for all four samples. The shift in the spectra between different samples is clearly seen in this figure, with luminescence energy increasing with increasing average isotopic mass of gallium. The eight components of the spectra in this figure all have characteristic energies which were measured using a curve fit to the spectral line from which the line center can be acquired. The characteristic energies of each line and the shift of each line relative to the same line in ^{69}GaP is given in Table 4.1. The stated results of bandgap shift are to be chosen such that the measured shift of all components is within the uncertainty of the bandgap shift. It is confidently stated that the spectral shift relative to ^{69}GaP is (+0.8 ± 0.1)cm^{-1} for the ^{nat}GaP, (+2.0 ± 0.1)cm^{-1} for the ^{anti}GaP and (3.05 ± 0.1)cm^{-1} for the ^{71}GaP.

These results are further analyzed by plotting the bandgap shift versus average isotopic mass as in Fig 4.2. A linear least squares fit to the slope of the line gives the change in bandgap with respect to a change in average isotopic mass of gallium, $dE_0/d\langle M_{Ga}\rangle$ = 1.55(7)cm^{-1}/amu = 0.19(1)meV/amu. From this then the cation contribution to the zero point renormalization of the bandgap, ΔE_o^c, may be calculated from

$$\Delta E_o^c = -2\langle M_{Ga}\rangle \, dE_0/d\langle M_{Ga}\rangle = -216(10)\text{cm}^{-1} = -27(2)\text{meV}$$

Where we have used the average isotopic mass of natural gallium, $\langle M_{Ga}\rangle$ = 69.72amu.

The total zero point renormalization of the bandgap, ΔE_o, has already been estimated as ΔE_o = -86meV in a previous study[14] using the temperature dependence of the bandgap. This estimate of the total zero point renormalization can be used to further estimate the anion contribution to the zero point renormalization, ΔE_o^a, as the difference between the total and the cation contribution,

$$\Delta E_o^a = \Delta E_o - \Delta E_o^c = -59\text{meV}.$$

4.2 Conclusions

Luminescence spectra of the sulfur-donor carbon-acceptor pair band for samples of GaP with differing gallium isotopic composition have been observed. Measurements of the shift in these optical spectra have been presented. The measurements of shift in optical spectra is found to be consistent between different components of the fine structure in these spectra. The indirect bandgap dependence on gallium isotopic mass has been calculated. These results are understood in the context of the renormalization of the bandgap due to the electron-phonon interaction.

Further estimates of the cation and anion contributions to the zero point renormalization of the bandgap are also calculated. These estimates support the conclusion that there is a greater isotope dependence of the bandgap upon the lighter of the two atoms in a binary compound semiconductor and that the vibrations of the lighter atom contribute more to the zero point renormalization of the bandgap.

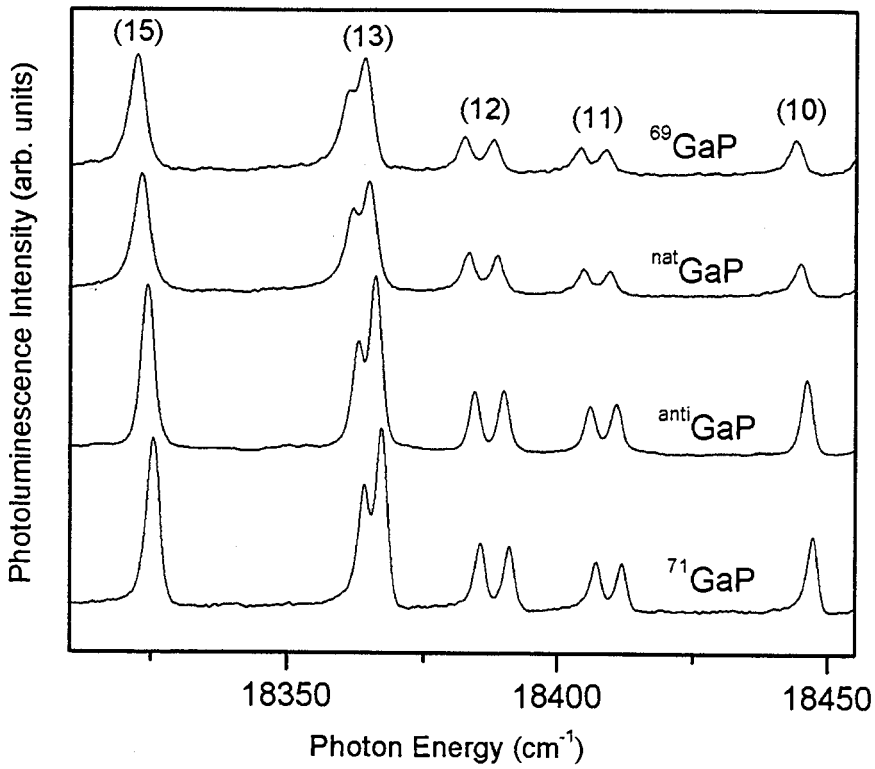

Figure 4.1 Photoluminescence spectra of the four GaP samples are shown in the spectral region covering the (10) through (15) shells of the discrete sulfur-donor carbon-acceptor pair transitions.

Shell No	Energy of Line Center Minus 18300 (cm^{-1})				Shift relative to ^{69}GaP (cm^{-1})		
	^{69}GaP	^{nat}GaP	^{anti}GaP	^{71}GaP	^{71}GaP	^{nat}GaP	^{anti}GaP
10	144.07	144.92	146.1	147.13	3.06	0.85	2.03
11a	104.12	104.86	106.1	107.19	3.07	0.74	1.98
11b	108.87	109.65	110.88	111.9	3.03	0.78	2.01
12a	82.53	83.3	84.52	85.58	3.05	0.77	1.99
12b	87.87	88.69	89.94	90.96	3.09	0.82	2.07
13a	61.1	61.93	62.99	64.18	3.08	0.83	1.89
13b	64.28	65.11	66.22	67.36	3.08	0.83	1.94
15	22.28	23.15	24.38	25.42	3.14	0.87	2.1
				Average Shift	3.075	0.811	2.001

Table 4.1 Experimentally obtained results of the line centers for shells (10) through (15) of the sulfur-donor carbon-acceptor pair band in the four different GaP samples. The shift indicates the difference in energy of the line centers between the ^{69}GaP sample and the other three samples.

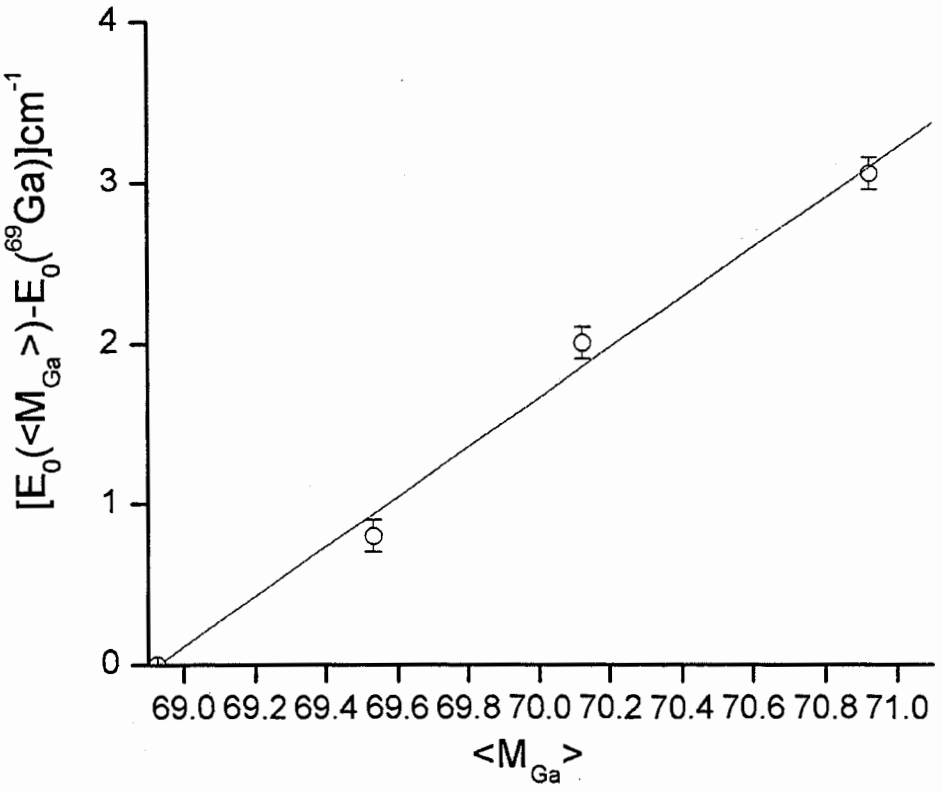

Figure 4.2 Shift of the indirect ($\Gamma \rightarrow \Delta$) gap of GaP vs. average isotopic mass of gallium. This plot yields slope 1.55(7) cm^{-1}/amu = 0.19(1) meV/amu.

Chapter 5 : CdS Results

5.1 Photoluminescence

The photoluminescence due to bound exciton recombination in CdS has been well documented in the past[15,16] . In this thesis we will use the same formalism for the fine structure of these spectra as has been used in Ref. 15. The recombination luminescence for excitons bound to neutral donors is dominated by the I_2 line, and a series of lines at higher energy. The I_2 line represents the recombination of the exciton in its ground state and a neutral donor left behind with its valence electron in the ground state. The higher energy lines(I_2^z and I_2^a) represent recombination from donor bound exciton excited states.

The photoluminescence spectra of these transitions is shown in Fig 5.1 for both the natural CdS sample and the $Cd^{34}S$ sample. A visible shift between the two spectra is noted with the energy of the transitions being greater for the $Cd^{34}S$ sample. The line centers were measured using a curve fit program and the resulting shift between the two samples is given in Table 5.1. The three bound exciton transitions all give an energy shift within limits $10.6cm^{-1} \leq \Delta E \leq 11.1cm^{-1}$.

Some of the free exciton transitions were also observed with photoluminescence spectroscopy. In Fig 5.1 the $A_{n=1}(\Gamma_{5L})$ transition line is present, so a similar measurement of the shift was done and is given in Table 5.1. The $A_{n=2}$ and $A_{n=3}$ free exciton transition lines are seen in the photoluminescence spectra of Fig. 5.2. These spectra were collected with the emitted light polarized such that $\mathbf{E} \| \mathbf{c}$. Related $A_{n=2}$ and $A_{n=3}$ photoluminescence lines are seen in Fig 5.3 where the emitted light is polarized such that $\mathbf{E} \perp \mathbf{c}$. In both polarizations the $A_{n=2}$ line has a stronger intensity which reduces uncertainty in the

measurement of its shift. All of the measured shifts in the free and bound exciton lines have been listed in Table 5.1. The $A_{n=2}$ line has a shift consistent with the $A_{n=1}$ shift and both are consistent with the bound exciton line shifts. The shift of the $A_{n=3}$ transition is also consistent with the other measured shifts for both polarizations, although $A_{n=3}$ has a higher uncertainty which is indicative of the difficulty in measurement with its weak line intensity.

5.2 Reflectance Spectroscopy

Reflectance spectra were collected over the excitonic-polariton region in CdS for both the $Cd^{nat}S$ and $Cd^{34}S$ samples. Studies of reflectance spectroscopy in this region have already been well documented[17,18] using a formalism that will be adopted in this thesis. The spectra were collected in both polarizations of incident light because the difference in selection rules for the two polarizations leads to the presence of different fine structure.

The reflectance spectrum for the $\mathbf{E} \| \mathbf{c}$ polarization is shown in Fig. 5.4 where it is seen that the $B_{n=1}(\Gamma_1)$ and $B_{n=2}$ signatures are both present. A higher energy portion of this spectrum is shown in Fig. 5.5 which contains the $C_{n=1}(\Gamma_1)$ free exciton feature. The measured shifts for all of these transitions is given in Table 5.1.

The reflectance spectrum for the $\mathbf{E} \perp \mathbf{c}$ polarization is shown in Fig. 5.6 where it is seen that the $A_{n=1}(\Gamma_{5L})$, $A_{n=2}$, $B_{n=1}(\Gamma_{5L})$ and $B_{n=2}$ excitonic-polariton signatures are all present. The measured shifts for all of these features are stated in Table 5.1. For all of the measured shifts presented in Table 5.1 pertaining to the reflectance data a similar trend is found in the uncertainty of measurement as was found for the photoluminescence data. The stronger intensity transitions have a smaller uncertainty of measurement due to the ease with which one may measure a stronger feature. The shifts for the $A_{n=2}$ and $A_{n=3}$

reflectance features in $\mathbf{E}\perp\mathbf{c}$ polarization, along with the shifts for the $B_{n=2}$ and $C_{n=1}(\Gamma_1)$ features in the $\mathbf{E}\parallel\mathbf{c}$ polarization all have high uncertainty of measurement due to the weak intensity of these features. The $C_{n=1}(\Gamma_1)$ feature has an especially low signal to noise ratio, and large inherent width resulting in an especially high uncertainty.

5.3 Absorption Spectroscopy

The only absorption feature noted in this study is the $A_{n=1}(\Gamma_6)$ free exciton line. This feature is present in the reflectance spectra of Fig5.4 where the incident light is polarized $\mathbf{E}\parallel\mathbf{c}$. This absorption takes place in reflectivity spectroscopy because the transmitted light is partially reflected off the back surface of the sample and collected by the spectrometer. The sample is thick enough to allow the back-reflected light to traverse a distance long enough that absorption could become significant. This absorption feature has previously been documented in the literature[19]. This absorption line is very sharp, so its shift was measured between samples with a low uncertainty. This shift is given in Table 5.1.

5.4 Bandgap Shift

The stronger features of the reflectance spectra, comprising of $A_{n=1}(\Gamma_{5L})$, $B_{n=1}(\Gamma_1)$ and $B_{n=1}(\Gamma_{5L}+\Gamma_{5T})$, along with the stronger intensity photoluminescence free exciton transition lines, comprising of $A_{n=1}(\Gamma_{5L})$ and $A_{n=2}$ transitions, all have shift measurement with uncertainty $\leq 0.4\text{cm}^{-1}$. These measured shifts all fall within the range $10.6\text{cm}^{-1} \leq \Delta E \leq 11.3\text{cm}^{-1}$.

The measured shift in free exciton related transitions is indicative of the shift in the electronic bandgap. The shift in the free exciton energies should closely follow the isotopic shifts in the band gap energy, except for a possible dependence of the free

exciton binding energy on the isotopic mass, which is expected to be small. The bound exciton transitions could have a small dependence of the exciton localization energy upon isotopic mass. So the measured shifts in the bound exciton transitions is not as trustworthy an indication of the bandgap shift as for shifts in free exciton related transitions. With this reasoning in mind, the stated result of measured bandgap shift is chosen from the measured shifts of free exciton related spectra. This being said, the shift in the direct bandgap of CdS is confidently stated as $10.9(2)cm^{-1} = 1351(25)\mu eV$ for a change in sulfur average isotopic mass of $\Delta\langle M_S\rangle = 1.895amu$.

This result may be contrasted with the findings of Ref. 20 where it is observed that the shift due to change in sulfur isotope mass is $12cm^{-1}$. A possible explanation for why this result is greater than ours is in the isotopic purity of the samples used. In both studies, isotopically pure ^{34}S was used for one sample. For the second sample, we used natural S (95% ^{32}S) whereas isotopically pure ^{32}S was used in the other study. This makes for a greater change in sulfur mass between samples in the earlier study and a resulting greater observed shift in optical spectra between samples.

In Ref. 20 there is further reporting of the observed isotope shifts of the excited state free exciton transitions. Namely, for the $A_{n=2}$ and $B_{n=2}$ free exciton excited states, a reported shift of the optical spectra is given as $\sim 3cm^{-1}$. This is far less than the reported shift of the ground state free exciton optical spectra, mentioned above. This lead the authors to conclude that the free exciton binding energy shows isotopic dependence and that the bandgap energy does not. The present results are in conflict with this claim. We report that the excited state free exciton spectra and the ground state free exciton spectra shift equivalently due to change in sulfur isotope mass, and we report no observable

isotopic dependence of the free exciton binding energy. The consistency of shifts of different optical spectra reinforce our assumption that the bandgap is the predominant mechanism of isotopic dependence.

Our results may be used to calculate the sulfur isotope dependence of the direct bandgap energy of CdS. The change in average sulfur isotopic mass between the $Cd^{nat}S$ ($\langle M_S \rangle$ = 32.0625amu) and $Cd^{34}S$ ($\langle M_S \rangle$ = 33.957amu) samples yields a shift of the direct bandgap with sulfur isotopic mass of $dE/d\langle M_S \rangle$ = 713(14)μeV/amu. This result compares well with the calculation of Ref. 21 where a two oscillator model is used to describe the bandgap shift observed under cadmium isotopic substitution in CdS. This model predicts the shift of the bandgap with isotopic mass of cadmium and sulfur, which proves to be different for A and B bandgaps. These predictions produce a value of $dE/d\langle M_S \rangle$ = 950μeV/amu (724μeV/amu) for the A (B) bandgap.

These predictions are in satisfactory agreement with our result, however in our findings we do not note any substantial difference in the shifts of A band edge related spectra and that of B band edge related spectra.

5.5 Conclusions

Luminescence spectra of the bound and free exciton regions and reflectivity spectra of the excitonic-polariton region of CdS have been observed in samples with differing sulfur isotopic composition. The shift in fine structure of these spectra between the different samples is found to be consistent amongst bound and free exciton and excitonic-polariton structure. With this consistency, it is concluded that the shift in optical spectra is due to isotopic dependence of the direct bandgap and that there is no observable changes due to isotopic dependence of the exciton binding energy. From the measured shifts in the

optical spectra, the shift in the direct bandgap of CdS due to change in sulfur isotope mass, ΔE, is estimated.

The sulfur isotopic dependence of the bandgap, $dE/d\langle M_S \rangle$, is calculated and found to agree with the estimates of Ref. 20 who used a two oscillator model to predict the sulfur and cadmium isotope dependence of the bandgap for band edges A and B. Our results do not reveal any difference in the bandgap shift for the different band edges A, B and C.

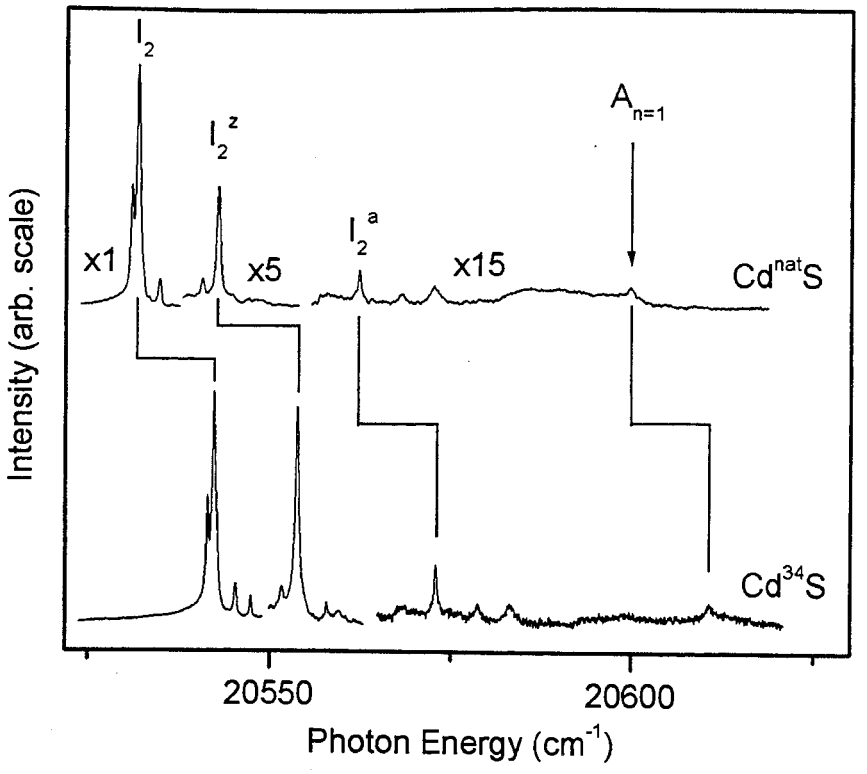

Figure 5.1 Photoluminescence of the bound and free exciton region in $Cd^{nat}S$ and $Cd^{34}S$. Three separate regions of the spectra have intensity magnified by a factor shown as **x**(factor). Inset broken lines indicate the shifts of spectral components between the two samples.

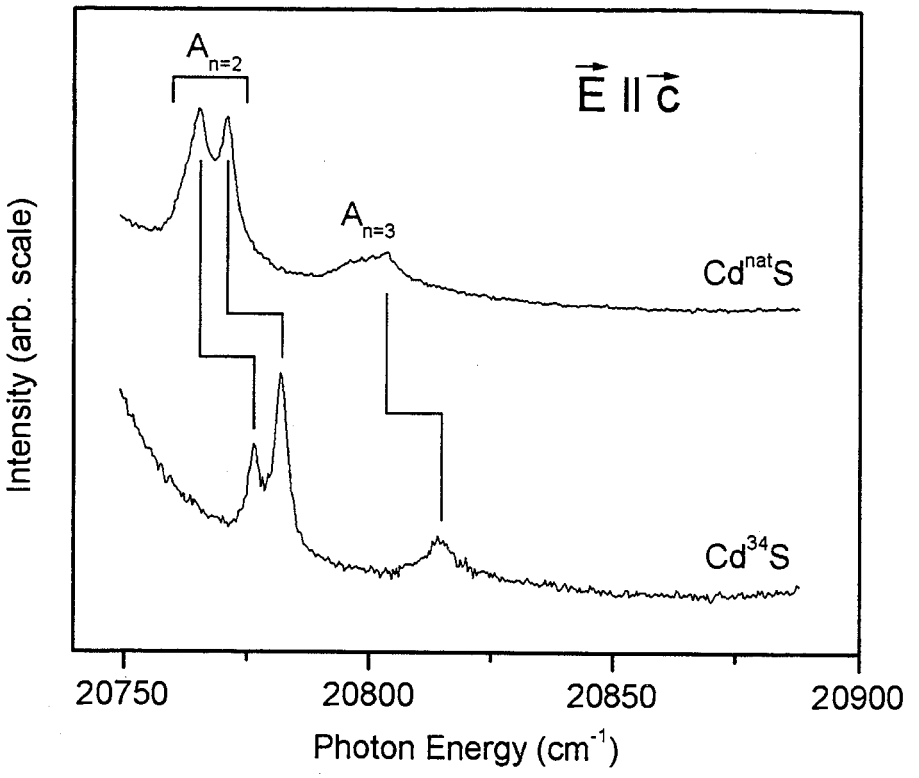

Figure 5.2 Photoluminescence in the free exciton region of $Cd^{nat}S$ and $Cd^{34}S$. Excitation light is polarized with $\mathbf{E} \| \mathbf{c}$. Inset broken lines indicate the shifts of spectral features between the two samples.

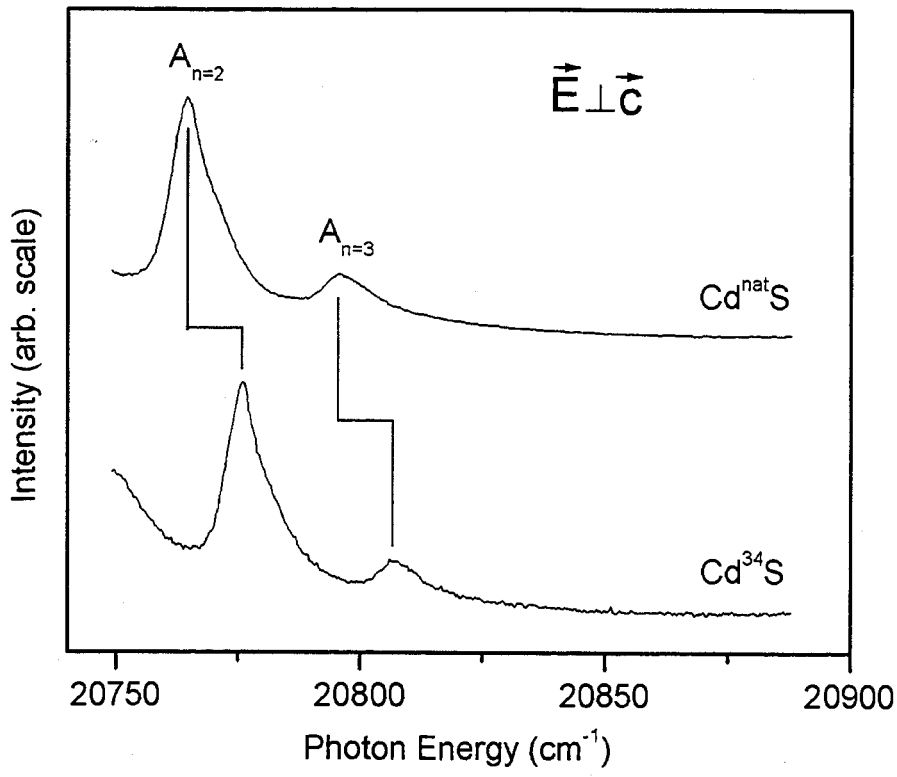

Figure 5.3 Photoluminescence in the free exciton region of $Cd^{nat}S$ and $Cd^{34}S$. Excitation light is polarized with **E⊥c**. Inset broken lines indicate shifts in spectral components between the two samples.

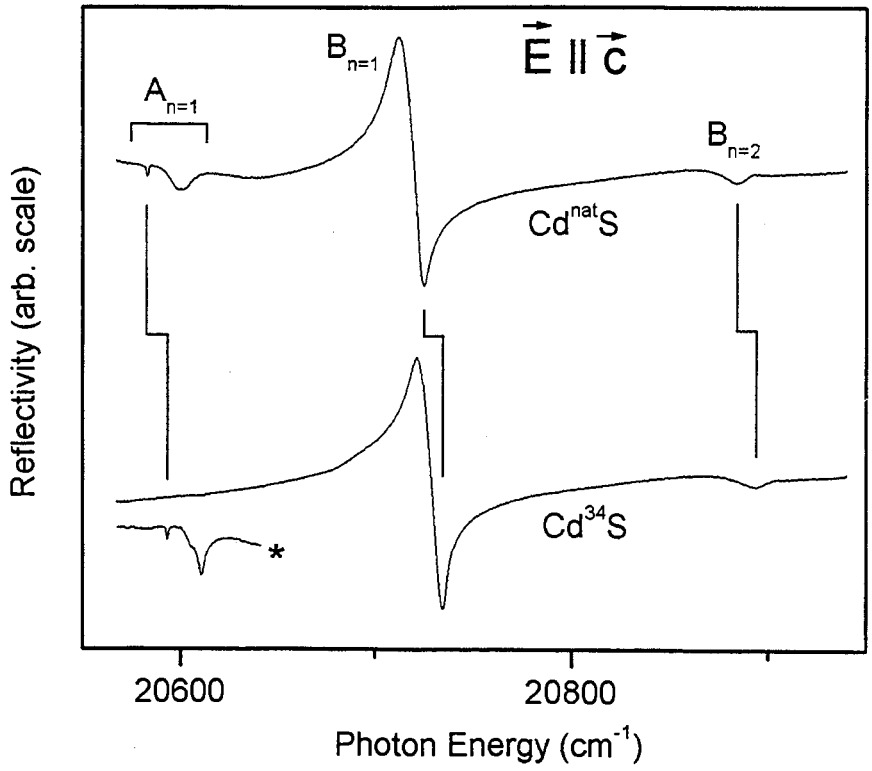

Figure 5.4 Reflectance spectra collected in the excitonic-polariton region of $Cd^{nat}S$ and $Cd^{34}S$. Emitted light polarized with $\mathbf{E} \| \mathbf{c}$. Inset broken lines indicate shifts in spectral components between the two samples. Due to the light polarization, only the Γ_1 component of the $B_{n=1}$ and $B_{n=2}$ transitions is allowed. The $A_{n=1}$ fine structure absorption feature is present with an inset broken line indicating the shift of its Γ_6 component. *Inset spectra of $Cd^{34}S$ with sample thickness enough to allow absorption.

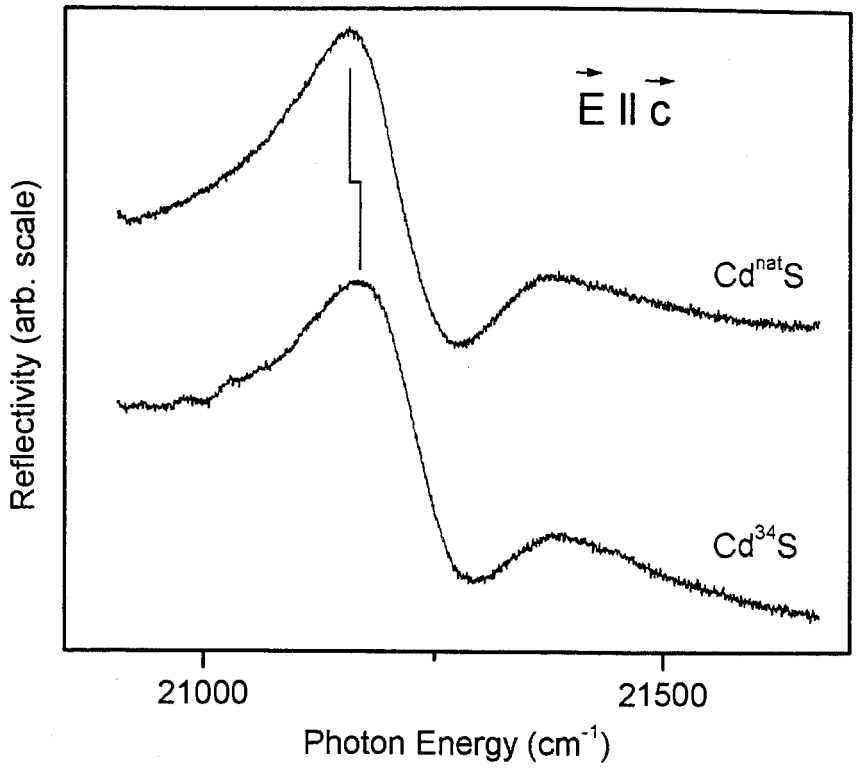

Figure 5.5 Reflectivity of the C edge excitonic-polariton region in $Cd^{nat}S$ and $Cd^{34}S$. Emitted light is polarized with $\mathbf{E} \| \mathbf{c}$. Inset broken line indicates the shift in spectral components between the two samples.

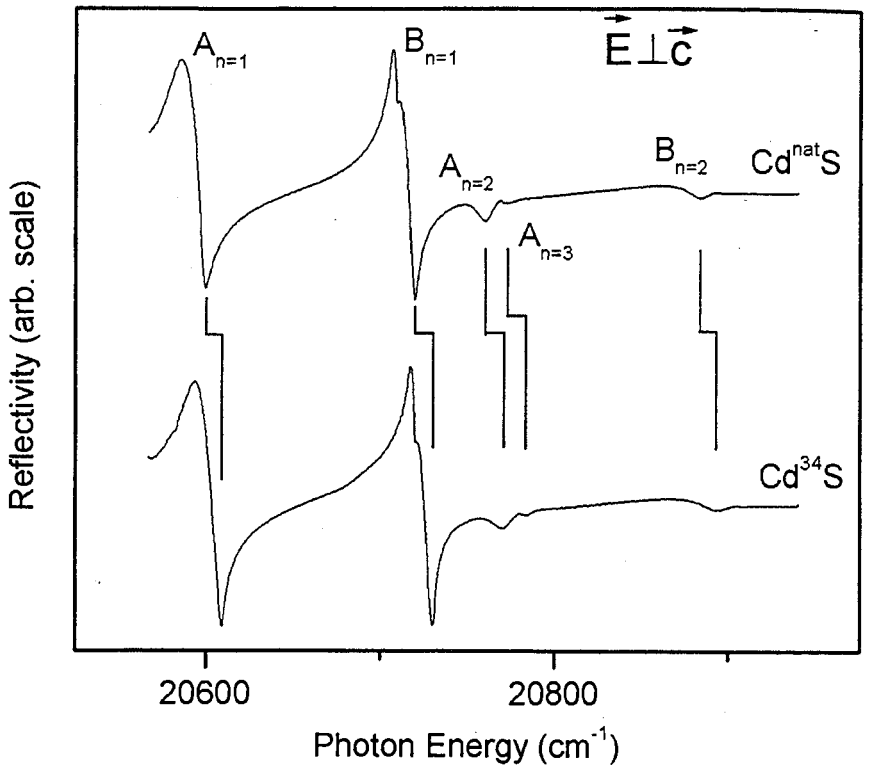

Figure 5.6 Reflectivity of the excitonic-polariton region of $Cd^{nat}S$ and $Cd^{34}S$. Emitted light polarized with **E⊥c**. Inset broken lines indicate shifts in spectral components between the two samples. Due to the light polarization, only the Γ_5 component of the $B_{n=1}$ and $B_{n=2}$ transitions is allowed. Similarly, only the Γ_{5L} component of the $A_{n=1}$ transition is allowed.

Transition	Method	ΔE_o (cm^{-1})
I_2	PL	10.6 ± 0.1
I_2^z	PL	11.1 ± 0.1
I_2^a	PL	10.6 ± 0.1
$A_{n=1}$ (Γ_6)	A ‖	10.8 ± 0.2
$A_{n=1}$ (Γ_{5L})	PL	11.0 ± 0.2
$A_{n=1}$ (Γ_{5L})	R ⊥	10.9 ± 0.2
$A_{n=2}$	PL ‖	11.3 ± 0.4
$A_{n=2}$	PL ⊥	11.1 ± 0.4
$A_{n=2}$	R ⊥	10.2 ± 0.5
$A_{n=3}$	PL ‖	11.8 ± 1.1
$A_{n=3}$	PL ⊥	10.9 ± 0.6
$A_{n=3}$	R ⊥	10.7 ± 0.6
$B_{n=1}$ (Γ_1)	R ‖	10.9 ± 0.3
$B_{n=1}$ ($\Gamma_{5L}+\Gamma_{5T}$)	R ⊥	10.6 ± 0.4
$B_{n=2}$	R ‖	9.4 ± 1.1
$B_{n=2}$	R ⊥	9.8 ± 1.2
$C_{n=1}$ (Γ_1)	R ‖	15 ± 6
$C_{n=1}$ (Γ_5)	R ⊥	14 ± 5

Table 5.1 Measured energy shifts for listed spectral components taken as $\Delta E_o = E_0(Cd^{34}S) - E_0(Cd^{nat}S)$. Methods used are photoluminescence(PL), reflectivity(R) and absorption(A) with parallel(‖) and perpendicular(⊥) signs indicating the orientation of the **E** axis relative to the **c** axis.

References

[1]M. Cardona, Phys. Stat. Sol. B **220**, 5 (2000).

[2]E.E. Haller, J. Appl. Phys. **77**, 2857 (1995).

[3]www.npl.co.uk/mass/avogadro

[4]C. Kittel, *Introduction to Solid State Physics* (3rd edition), John Wiley & Sons, New York, 1967.

[5]E.L. Ivchenko, *Excitons*, edited by M.D. Sturge and E.I. Rashba, North-Holland, 141 (1982).

[6]P.J. Dean, *Progress in Solid State Chemistry*, edited by J.D. McCaldin and G. Somorjai, Pergamon (1973), Vol. 8, p. 1.

[7]F. Williams, Phys. Stat. Sol. **25**, 493 (1968).

[8]J.D. Wiley and J.A.Seman, Bell Sys. Tech. J. **50**, 355 (1970).

[9]D.G. Thomas, M. Gershenzon and F.A. Trumbore, Phys. Rev. **133**, A269 (1964).

[10]C.W. Litton, D.C. Collins and T.C. Collins, Phys. Rev. **B6**, 2269 (1972).

[11]D. Auvergne, P. Merle and H. Mathieu, Phys. Rev. **B12**, 1371 (1975).

[12]M. Cardona, Phys. Stat. Sol. A **188**, 1209 (2001).

[13]E. Hecht, *Optics* (2nd edition), Addison-Wesley, 425 (1987).

[14]R. Pässler, Phys. Stat. Sol. **216**, 975 (1999). Zero-point gap renormalizations are obtained with the expression $\Delta E_0 = \alpha\Theta_p/2$ where the fit parameters α and Θ_p are listed in Table I of this reference.

[15]J. Gutowski, Solid State Comm. **58**, 523 (1986).

[16]H. Malm and R.R. Haering, Can. J. of Phys. **49**, 2432 (1971).

[17]D.G. Thomas and J.J. Hopfield, Phys. Rev. **116**, 573 (1959).

[18]D.G. Thomas and J.J. Hopfield, Phys. Rev. **128**, 2135 (1962).

[19]J.J. Hopfield, D.G. Thomas, Phys. Rev. **122**, 35 (1961).

[20]F.I. Kreĭngol'd, K.F. Lider, and M.B. Shabaeva, Fiz. Tverd. Tela (Leningrad) **26**, 3940 (1984) [Sov. Phys. Solid State **26**, 2102 (1985)].

[21]J.M. Zhang, T. Ruf, R. Lauck, and M. Cardona, Phys. Rev. B **57**, 9716 (1998).